JOURNAL OF MATERIALS SCIENCE 28 (1993) 3283–3290

# Textures of tantalum metal sheets by neutron diffraction

C. S. CHOI
*Energetics and Warheads Division, ARDEC, Picatinny Arsenal, NJ 07806, USA and Reactor Radiation Division, National Institute of Standards and Technology, Gaithersburg, MD 20899, USA*

H. J. PRASK, J. OROSZ
*Reactor Radiation Division, National Institute of Standards and Technology, Gaithersburg, MD 20899, USA and Energetics and Warheads Division, ARDEC, Picatinny Arsenal, NJ 07806, USA*

The orientation distributions of six tantalum samples, TaPA, TaG1, TaG2, TaQ2-S1, TaQ2-S2 and TaQ2-S4, were studied by neutron diffraction and ODF analysis. The TaPA specimen is a commercial tantalum sheet with an unknown fabrication history. The TaG1 and TaG2 were fabricated from a powder metallurgical ingot by uniaxial compression, and the TaQ2 type samples were fabricated from commercial stock by similar uniaxial forging. TaQ2-S1 is the section closest to the centre of the forged disc, S2 is the intermediate section, and S4 is the section adjacent to the periphery. The texture of TaPA consisted of many components, including $\{0\,1\,4\}\langle 1\,0\,0\rangle$, $\{1\,1\,1\}\langle \bar{3}\,2\,1\rangle$, $\{1\,0\,0\}\langle 0\,1\,0\rangle$, and $[1\,1\,1]/[1\,0\,0]$ double-fibre textures with the fibre axes oriented parallel to the normal direction. The two TaG-type specimens were dominated by the $[1\,1\,1]/[1\,0\,0]$ double-fibre texture, accompanied by a weak $\{1\,0\,0\}\langle 0\,1\,0\rangle$ cube texture. The three sections of TaQ2 had much higher degrees of texture than the TaG-type samples, with an extremely strong (1 1 1) peak, which consists of $(1\,1\,1)\langle 1\,1\,\bar{2}\rangle$, $(1\,1\,1)\langle \bar{1}\,\bar{1}\,2\rangle$, and $[1\,1\,1]$ fibre texture. The average pole density of the three equivalent orientations of $(1\,1\,1)\langle 1\,1\,\bar{2}\rangle$ was the strongest for the S1 with over 150 multiples of random distribution (mrd), and gradually decreased with increasing radial distance to about 100 mrd for the S4 section. On the other hand, the average intensity of $(1\,1\,1)\langle \bar{1}\,\bar{1}\,2\rangle$ type orientations was increased from about 40 mrd at S1 to about 100 mrd for the S4 section.

## 1. Introduction

Tantalum is a heavy metal with a high melting point, high ductility, and moderate tensile properties. Recently, this material has attracted considerable attention within the defense-related research community as a prime candidate material for armour penetrators. Numerous studies of the physical and mechanical properties of this material are underway by many investigators [1–3]. Because the physical and mechanical properties of polycrystalline materials are highly dependent on the crystallites orientation distribution, the performance of an armour penetration munition could be affected by the texture of the material.

Texture measurements are conducted most commonly by X-ray diffraction methods because of the easy availability and the faster measurement time compared to neutron diffraction. However, the penetration power of X-rays in the diffraction regime is so low in the heavy metals (approximately 1/10000 of that of neutrons) that it is essentially impossible to see non-destructively the subsurface texture below a few micrometres depth. The surface texture is often different from that of the interior, so that neutron diffraction was used in this study.

## 2. Samples

Six different samples, labelled TaPA, TaG1, TaG2, TaQ2-S1, TaQ2-S2 and TaQ2-S4, were prepared for this study. The TaPA specimen, with approximate dimensions of $5 \times 10 \times 10\ mm^3$ was cut from a long strip ($5 \times 18 \times 203\ mm^3$) of commercial tantalum sheet. The history of the fabrication process of the strip is unknown. We have assumed that the strip was fabricated by rolling along the long-axis direction (RD) of the original strip. The specimen was mounted on the diffractometer so that the normal direction (ND) to the sample surface was oriented parallel to the sample rotation axis.

The TaG1 and TaG2 specimens were fabricated from powder-metallurgically prepared cylindrical ingot by uniaxial compression along the cylinder axis direction, with 90% reduction at room temperature. The forged discs were annealed at 950 °C. Two pieces of square platelet specimens, $10 \times 10 \times 5\ mm^3$, were

cut from each sample, with one side of each square parallel to the radial direction of the forged disc. The two plates were glued together carefully to double the thickness (approximately cube shape) without disturbing their mutual orientation relationship.

The TaQ2 specimens were obtained from commercial vaccum-arc-cast ingot by using a similar fabrication process to that used for the TaG1 and TaG2 specimen, and annealed at slightly higher temperature. A 5 mm thick square disc of size 25 $\times$ 25 mm$^2$ was cut from the quarter section of the forged disc, in such a way that one of the diagonals of the square was aligned parallel to the radial direction (RD) of the forged disc. The square plate was cut further into four identical square sections with the dimensions of $12 \times 12 \times 5$ mm$^3$. Among the four, the two square sections contain the common radial line of the forged disc, each of which represents the section of the shortest and the longest radial distance, respectively. The section which is closer to the centre of the disc is labelled TaQ2-S1, the section at intermediate radial distance is TaQ2-S2, and the section at the furthest radial distance is labelled TaQ2-S4.

The term RD refers to the rolling direction for the TaPA sample and to the radial direction for the TaG- and the TaQ2-type samples. Similarly, the term TD refers to the transverse direction and to the tangential direction, respectively.

## 3. Experimental procedure

The samples were mounted on the four-circle neutron diffractometer at the NIST reactor. Each sample was mounted at the centre of the goniometer, with the ND oriented parallel to the sample rotation axis. The neutron beam with 0.118 nm wavelength from the (004) reflection of the graphite monochromator was used. The pole figure data of the five reflections, 200, 211, 220, 310 and 222, were measured over an entire orientation hemisphere ranging from 0–360° in $\phi$-angle and 90–0° in $\chi$-angle, each in 5° step intervals using the standard procedure [4].

The raw data were corrected for background neutrons. Absorption corrections were applied for the flat specimens, i.e. TaPA and the three TaQ2-type samples, assuming that the linear absorption coefficient is 0.146 mm$^{-1}$. The corrected data were converted to pole densities in multiples of the random distribution (mrd) units by normalizing them to the calculated powder diffraction intensity. The observed pole density data were smoothed by the Gaussian-filtering method with 1° width using the program popLA [5].

## 4. Orientation distribution function analysis

The orientation distribution function (ODF) analysis was performed using the program popLA developed

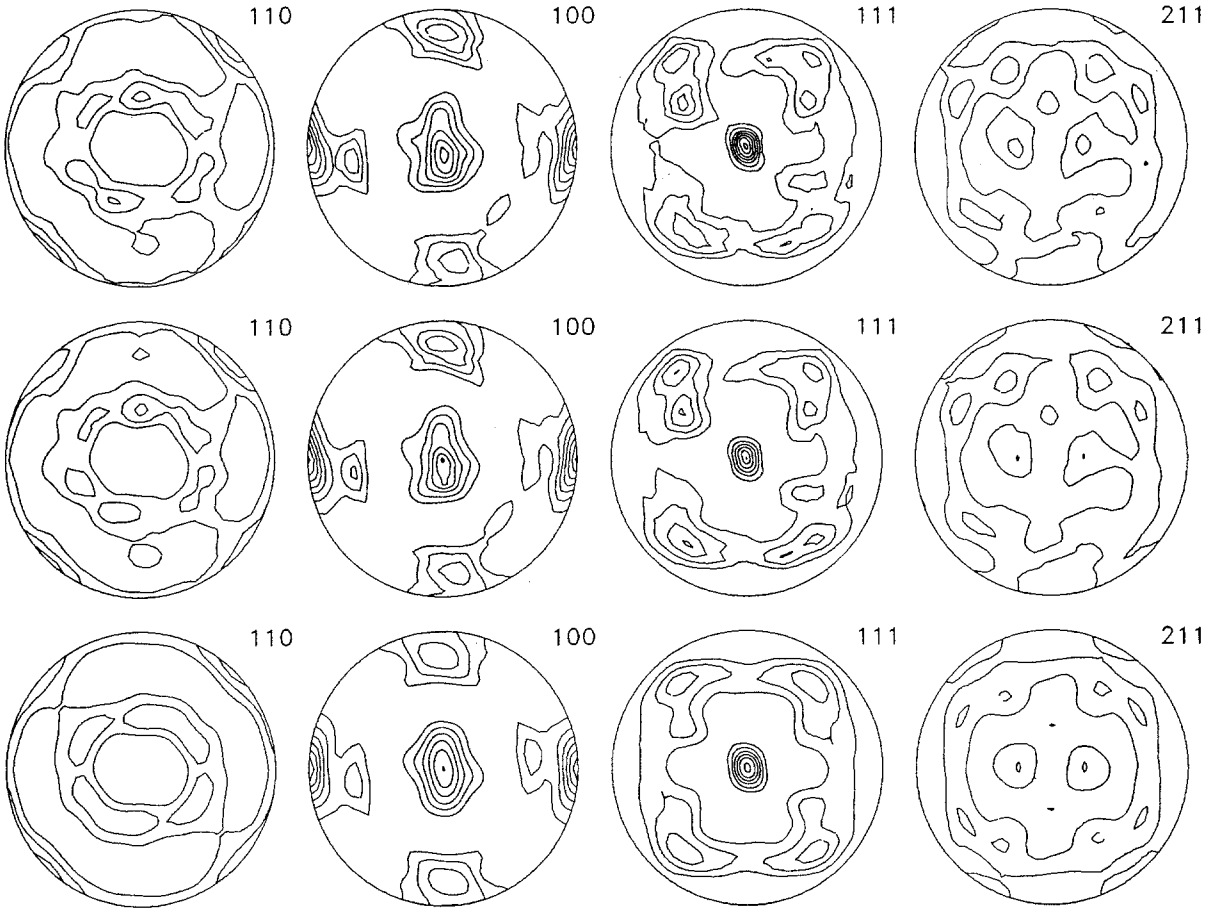


*Figure 1* Observed and recalculated pole figures of the TaPA sample. The figures on the top row are observed, those on the middle row are recalculated from the WIMV ODF, and those on the bottom row are from the Harmonic ODF. The contour levels of 1 mrd and higher are drawn in 0.5 mrd steps.

at Los Alamos National Laboratory [5]. popLA contains two ODF analysis programs, namely the WIMV and the harmonic method. Because the WIMV program used for this study has a limit of 25 in the total multiplicity, only four (1 1 0, 1 0 0, 1 1 1 and 2 1 1) out of the five experimental pole figures were used in the WIMV analysis. There are two different formalisms in the harmonic method, one by Bunge [6] and the other by Roe [7]. The program in popLA is based on the Roe formalism.

### 4.1 The ODF of TaPA

The ODF of TaPA was calculated by both methods. A triclinic sample symmetry was used because the pole figures did not show any higher symmetry. After 25 iterations, the RP error index, an integral relative error [8], was reduced to 1.1%. The recalculated pole figures from the WIMV ODF showed excellent agreement with the corresponding experimental pole figures, as compared in Fig. 1.

The ODF of the TaPA was analysed also by the harmonic method, using all five pole figures. A mirror symmetry perpendicular to the $z$-axis was imposed because the program had no triclinic sample symmetry option for the cubic crystal. In the pole figure, the mirror symmetry generates the two-fold rotation symmetry about the $z$-axis (centre of the pole figure) because of the inherent inversion symmetry of the sample orientation space. Therefore, all the recalculated harmonic pole figures in Fig. 1 exhibit two-fold rotation symmetry. Nevertheless, the agreement between the recalculated and the experimental pole figures was reasonably good.

The two sets of the three-dimensional sample orientation distributions (SOD) obtained from the two different ODFs were apparently similar, but the $\psi$-angular distribution of the harmonic ODF was distorted by the faulty two-fold symmetric constraint and the contour lines were smoother with slightly lower peak height than those of the WIMV ODF. Therefore, the WIMV ODF was chosen for the texture of TaPA. The WIMV SOD based on the Kocks-type [9] Euler angles are presented on the constant $\psi$-sections, as shown in Fig. 2. The SOD map exhibited several well-defined high-density tubes running parallel to the $\psi$-axis at the $\theta$–$\phi$ positions corresponding to 1 1 1, 0 1 4 (or 0 1 3), and 1 0 0 pole. The complete pole density distributions of the (1 1 1)$\langle uvw \rangle$, (0 1 4) $\langle uvw \rangle$ and (1 0 0)$\langle uvw \rangle$ tubes as a function of the $\psi$-angle were deduced from the SOD in following way. Firstly, the Euler angles corresponding to the ND orientation, $\theta$ and $\phi$, were calculated from the given $(hkl)$ using the orientation matrix. Then the pole density for the $\theta$–$\phi$ position at each $\psi$-section was determined from the SOD by linear interpolation. The resultant $\psi$-angular distributions of the (1 1 1)$\langle uvw \rangle$, (0 1 4)$\langle uvw \rangle$ and (1 0 0)$\langle uvw \rangle$ tubes are shown in Fig. 3.

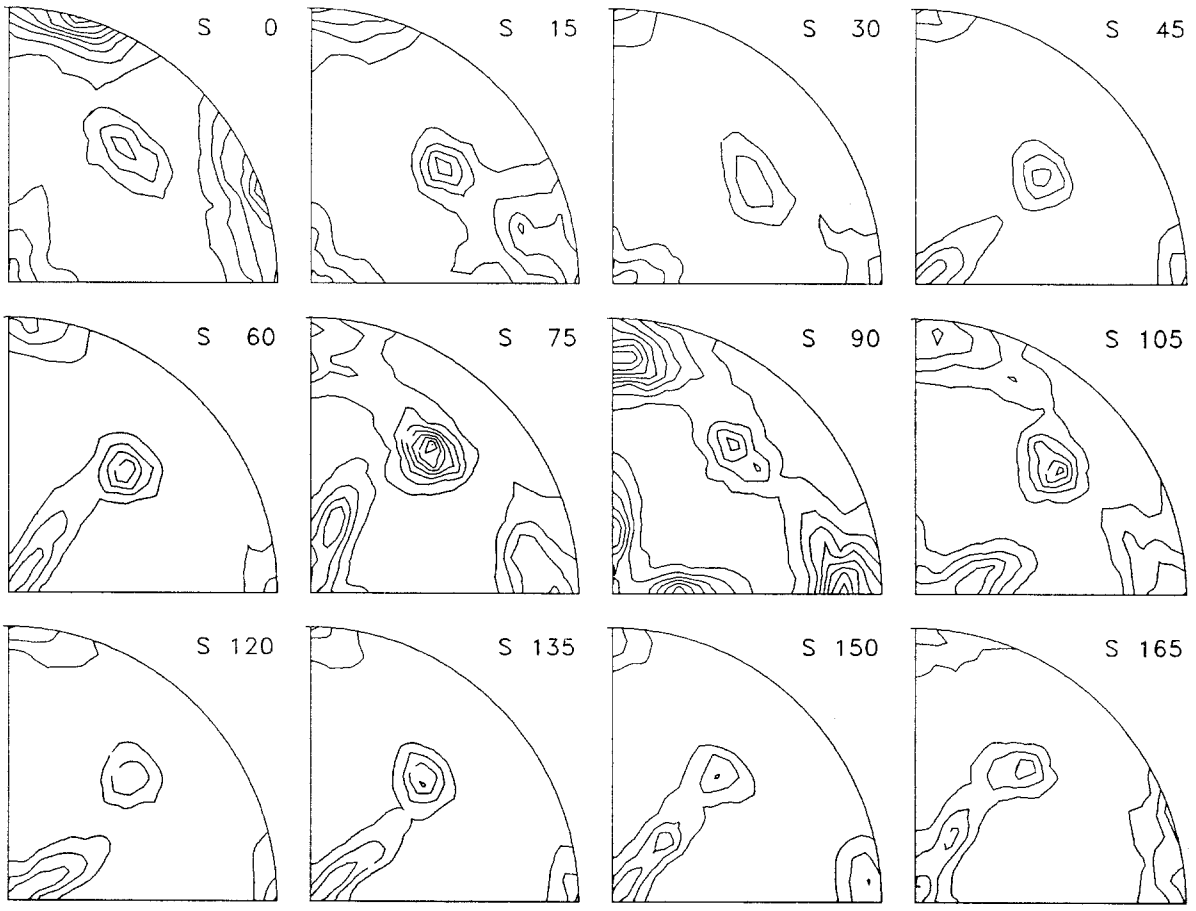


*Figure 2* The SOD of the TaPA sample, calculated from the WIMV ODF based on the Kocks Euler angles. The constant $\psi$ sections from $\psi = 0°$–$165°$ with $15°$ steps are presented in the crystal coordinates; 1 0 0 at the right edge, 0 1 0 at the top and 0 0 1 at the centre. The contour levels are given in 1 mrd steps.

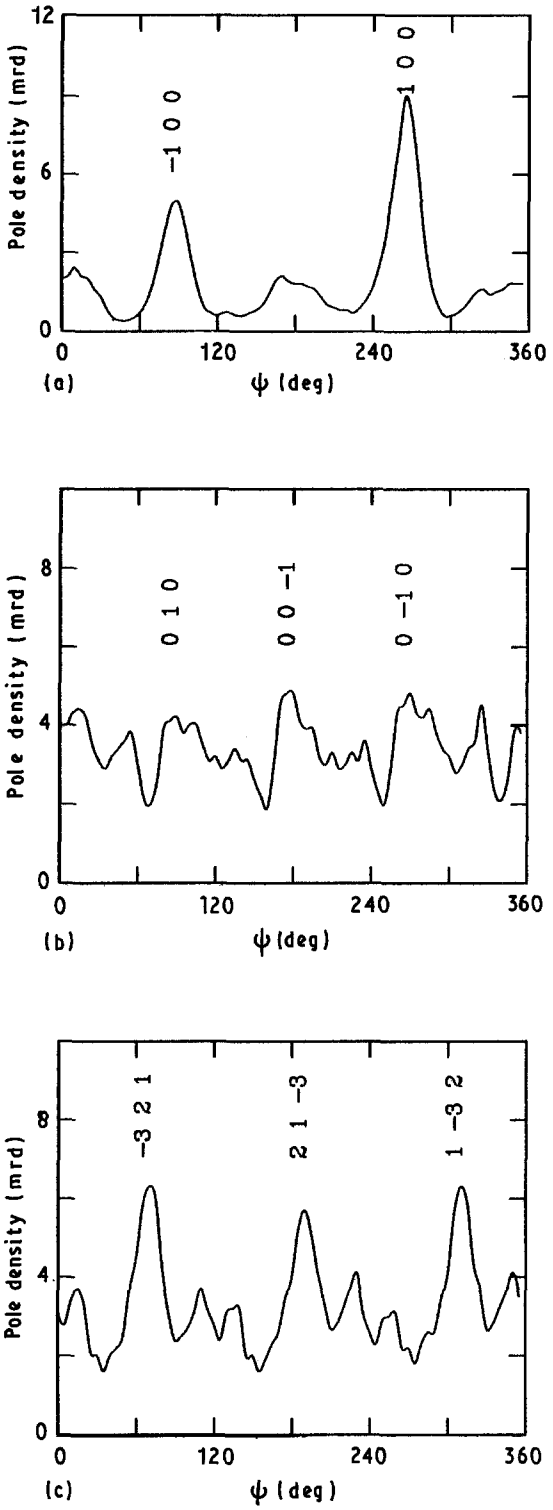


*Figure 3* The (a) (0 1 4) [$uvw$], (b) (1 0 0) [$uvw$] and (c) (1 1 1) [$uvw$] distributions of TaPA are presented as a function of the ψ-angles. The Miller indices of the [$uvw$] corresponding to the peak orientations in each distribution are included.

The (1 1 1)[$uvw$] distribution showed a total of twelve peaks which correspond to the equivalent orientations of the (1 1 1)⟨$\bar{3}$ 2 1⟩, (1 1 1)⟨$\bar{2}$ 3 $\bar{1}$⟩, (1 1 1)⟨$\bar{1}$ 3 $\bar{2}$⟩ and (1 1 1)⟨$\bar{3}$ 1 2⟩ type. Using the three-fold symmetric property of the (1 1 1)[$uvw$], the twelve orientations may be represented by four orientation types in the asymmetric unit. The pole densities of the four symmetry-independent orientations were quite different, with the strongest peaks (about 7 mrd) for the (1 1 1)⟨$\bar{3}$ 2 1⟩, and lesser intensity for the (1 1 1)⟨$\bar{2}$ 3 $\bar{1}$⟩, (1 1 1)⟨$\bar{1}$ 3 $\bar{2}$⟩ and (1 1 1)⟨$\bar{3}$ 1 2⟩ in order. The strongest orientations were labelled in Fig. 3. The (0 1 4)⟨$uvw$⟩ distribution showed strong (0 1 4)⟨1 0 0⟩ texture with an average intensity of 7 mrd, and smaller peaks at the (0 1 4)⟨0 $\bar{4}$ 1⟩ orientations. The (1 0 0)⟨$uvw$⟩ distribution showed a rather complicated profile, with the peak orientations spread over a wide range of the ψ-angles corresponding to the RD orientations of 0 4 1, 0 1 0, 0 4 $\bar{1}$, 0 2 $\bar{1}$, 0 3 $\bar{2}$, 0 1 $\bar{1}$ and 0 2 $\bar{3}$ (and their four-fold cyclic sets). This distribution could be characterized as an uneven [1 0 0] fibre with lesser density at the RD orientation near 0 3 1, 0 1 $\bar{3}$, 0 3 $\bar{1}$ and 0 $\bar{1}$ 3. The (1 1 1)⟨$uvw$⟩ distribution also had a constant base amount of about 2 mrd, which corresponds to the [1 1 1] fibre texture.

## 4.2. The ODF of TaG1 and TaG2

The experimental pole figures of the two TaG-type samples showed essentially an identical fibre-type texture with the fibre-axes oriented parallel to the ND. The triclinic sample symmetry was imposed in the WIMV analysis because of the slight deviation from the ideal fibre texture. After 22 iterations, the RP reduced to 1.2% for both TaG1 and TaG2. In the harmonic analysis, monoclinic sample symmetry was used for both samples. The recalculated pole figures obtained from the two ODFs both showed equally excellent agreement with the corresponding experimental pole figures for both samples, as can be seen in Fig. 4. Because the pole figures of the two samples were essentially identical, the pole figures of TaG2 are not shown in Fig. 4.

The two SODs obtained by the WIMV and the harmonic analysis were essentially identical for the TaG-type samples. The WIMV SODs were chosen in this study. The SODs of the TaG-type samples were consistent with the [1 1 1]/[1 0 0] double fibre texture with the fibre axes oriented parallel to the ND. The details of the (1 1 1) [$uvw$] and (1 0 0)[$uvw$] distributions obtained from each sample are shown in Fig. 5. The (1 0 0) [$uvw$] distributions revealed two texture components, [1 0 0] fibre and (1 0 0)⟨0 1 0⟩ cube texture. The fibre texture component of the distribution was about 7 mrd for both samples, and those of the cube textures were about 5 mrd for the TaG1 and about 12 mrd for the TaG2. The (1 1 1)[$uvw$] tube was found to be the [1 1 1] fibre texture, with an intensity of about 12 mrd for both samples.

## 4.3. The ODF of TaQ2

The pole figures of the three different sections of TaQ2 exhibit extremely well-developed textures with a pseudo three-fold rotation symmetry about the ND (centre of the pole figure) and a pseudo two-fold symmetry about the RD (3 o'clock direction), as shown in Fig. 6. The pole figures of the S2 section were omitted from the figure because of its similarity to those of the other sections. The ODF analyses were conducted by the WIMV method using the triclinic sample symmetry. The RP value of the S1 section was reduced to 1.5% after 27 iterative cycles, that of the S2

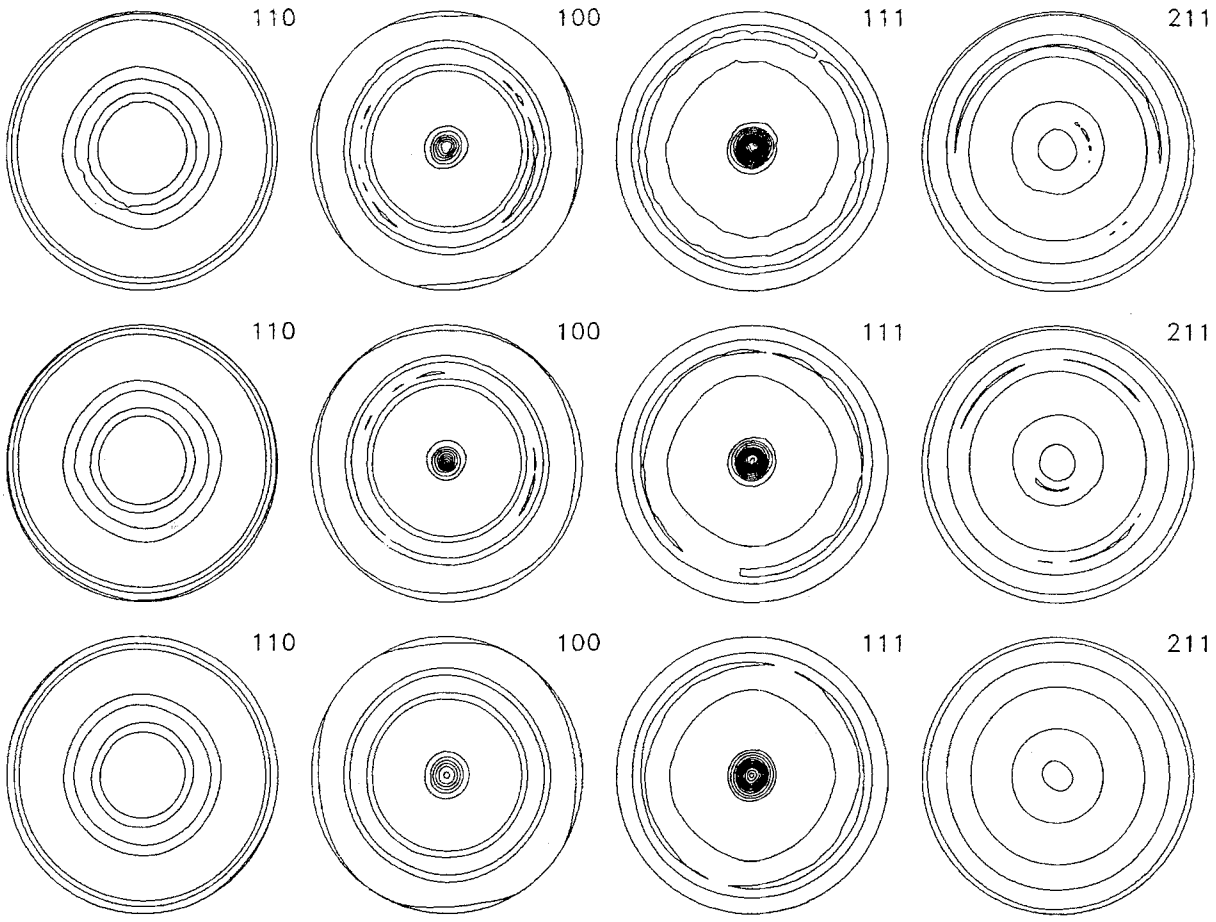


*Figure 4* Observed and recalculated pole figures of the TaG1 sample. The figures on the top row are observed, those on the middle row are recalculated from the WIMV ODF, and those on the bottom row are recalculated from the Harmonic ODF. The contour levels are given in 1 mrd steps.

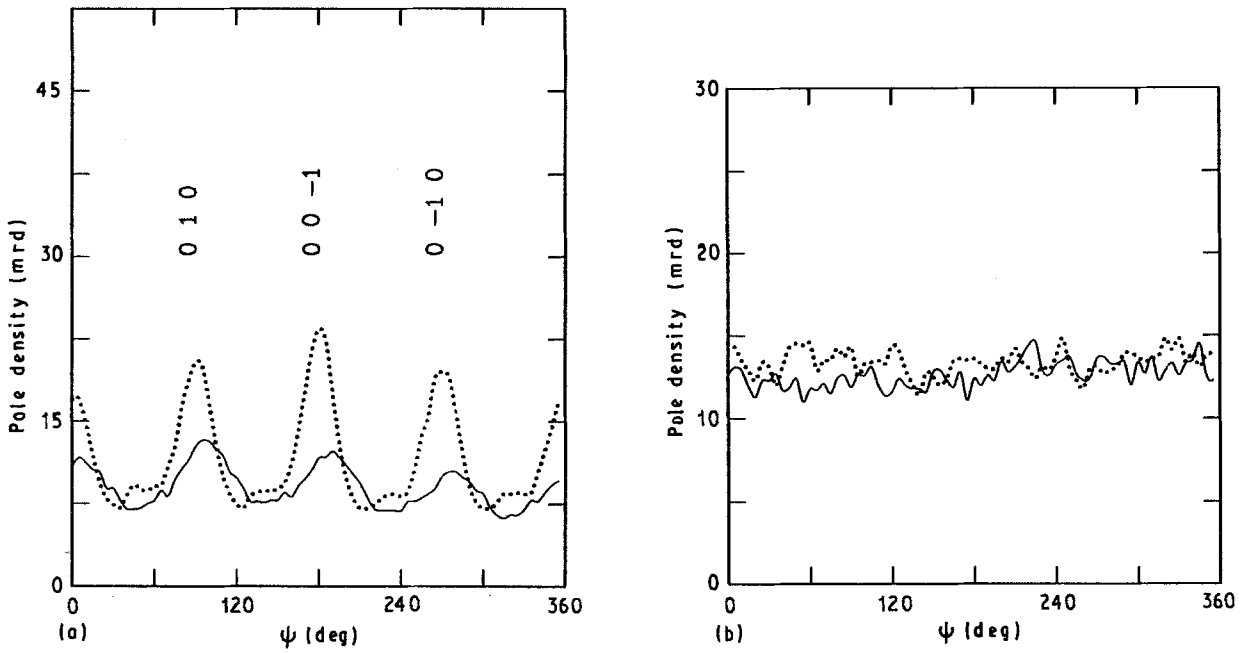


*Figure 5* The (a) (1 0 0) $[uvw]$ and (b) (1 1 1) $[uvw]$ distributions of the two TaG-type samples are presented as a function of the $\psi$-angles. The Miller indices of the $[uvw]$ corresponding to the peak orientations in the (1 0 0) $[uvw]$ distribution are included. (—) TaG1, (···) TaG2.

to 1.6% after 20 cycles, and that of the S4 to 1.7% after 21 cycles. The recalculated pole figures were essentially identical to the corresponding experimental pole figures of each sample, as compared in Fig. 6.

The SODs of the three sections showed extremely strong (1 1 1) $[uvw]$ tubes with the peak intensity higher than 100 mrd at some $\psi$-angles, and somewhat weaker $\{100\}$ $[uvw]$ tubes. The (1 1 1) $[uvw]$ and (1 0 0) $[uvw]$ distributions were obtained from the SOD of each sample, and are shown in Fig. 7. The dominant peaks in the (1 1 1) $[uvw]$ distribution were (1 1 1) $\langle \bar{2}\,1\,1 \rangle$ and its three-fold symmetric equivalent

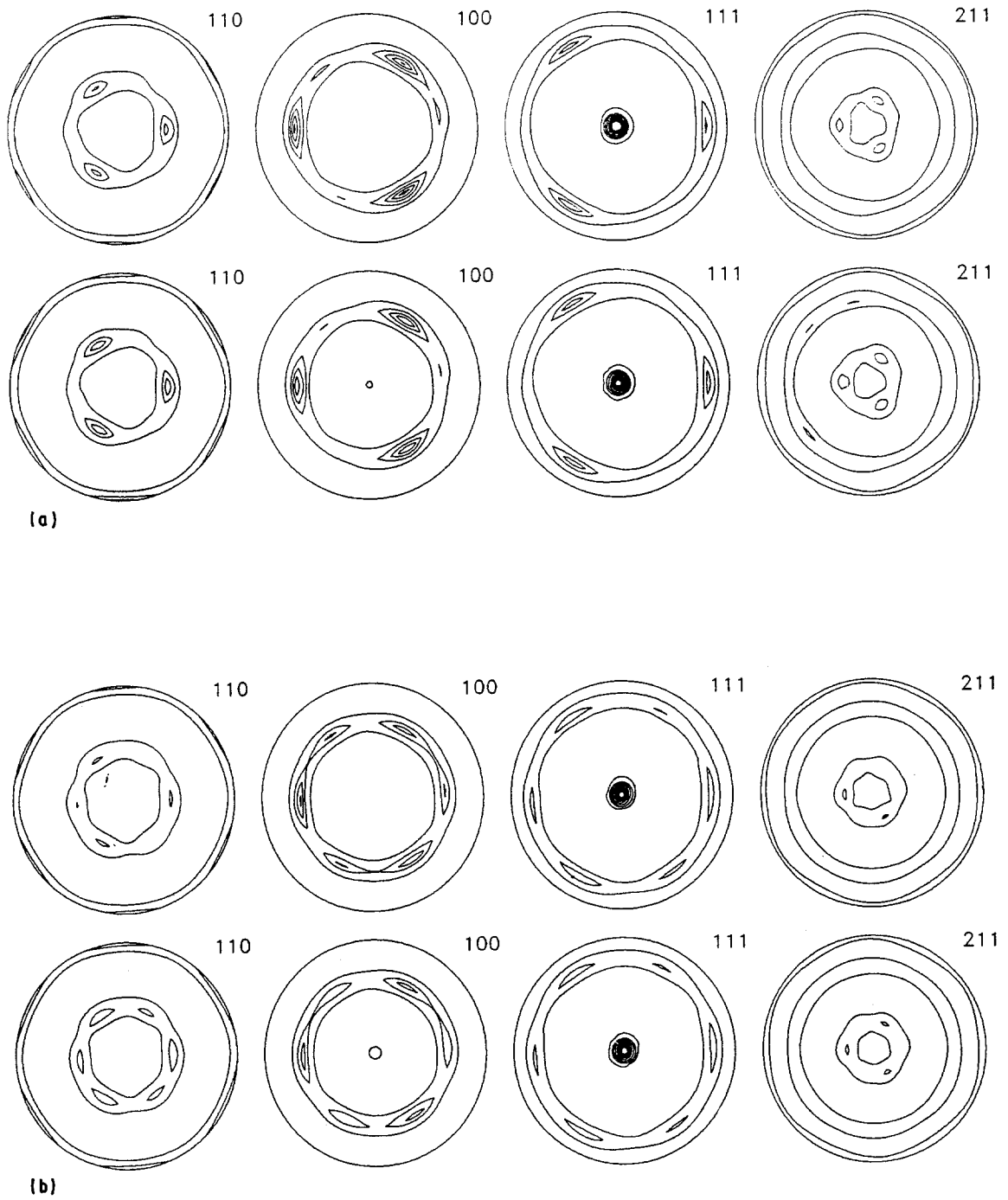


*Figure 6* Observed and recalculated pole figures of the (a) TaQ2-S1 and (b) TaQ2-S4 samples. In the figure for each sample, the pole figures on the top row are observed, those on the bottom row are recalculated from the WIMV ODF. The contour levels are given in 4 mrd steps, from 1 mrd up to 41 mrd.

orientations (cyclic permutation of the $uvw$ in the $(1\,1\,1)\langle uvw\rangle$). The orientation densities were the strongest for the S1 section with about 160 mrd, and decreased gradually with the increase of the radial distance to about 140 mrd for the S2 and to about 100 mrd for the S4, as shown in Fig. 7. The second most intense orientations in the distributions are the $(1\,1\,1)\langle 2\bar{1}\,1\rangle$ type orientations, which are distinguishable from the $(1\,1\,1)\langle\bar{2}\,1\,\bar{1}\rangle$ because of the absence of the two-fold symmetry for the [1 1 1] direction. The density of the $(1\,1\,1)\ \langle 2\bar{1}\,\bar{1}\rangle$type was about 40 mrd for the S1 section, and then increased to about 120 mrd for the S2 and about 80 mrd for the S4. Thus, the $(1\,1\,1)[uvw]$ distributions of the S1 (the section near the centre of the forged disc) exhibit a pseudo three-fold symmetry rather than the pseudo six-fold symmetry. The $(1\,1\,1)$ $[uvw]$ distribution of the S4 section exhibit comparatively less intensity fluctuation among the three sections, which suggests that the degree of fibre-texture is increasing with increase in the radial distance in the forged disc. The intensities of the fibre textures, estimated from the base heights of the distributions, are about 20 mrd for the S1 and S2 sections, and about 40 mrd for the S4.

The $(1\,0\,0)[uvw]$ tubes are much weaker than the $(1\,1\,1)\langle uvw\rangle$ tubes, and show fuzzy peak profiles with broad widths. The distribution of S1 section showed the intensity maximum near the $(1\,0\,0)\langle 0\,3\,2\rangle$, the S2 section near the $(1\,0\,0)\langle 0\,3\,1\rangle$, and the S4 had the maximum at the $(1\,0\,0)\langle 0\,1\,1\rangle$ orientation, as shown in

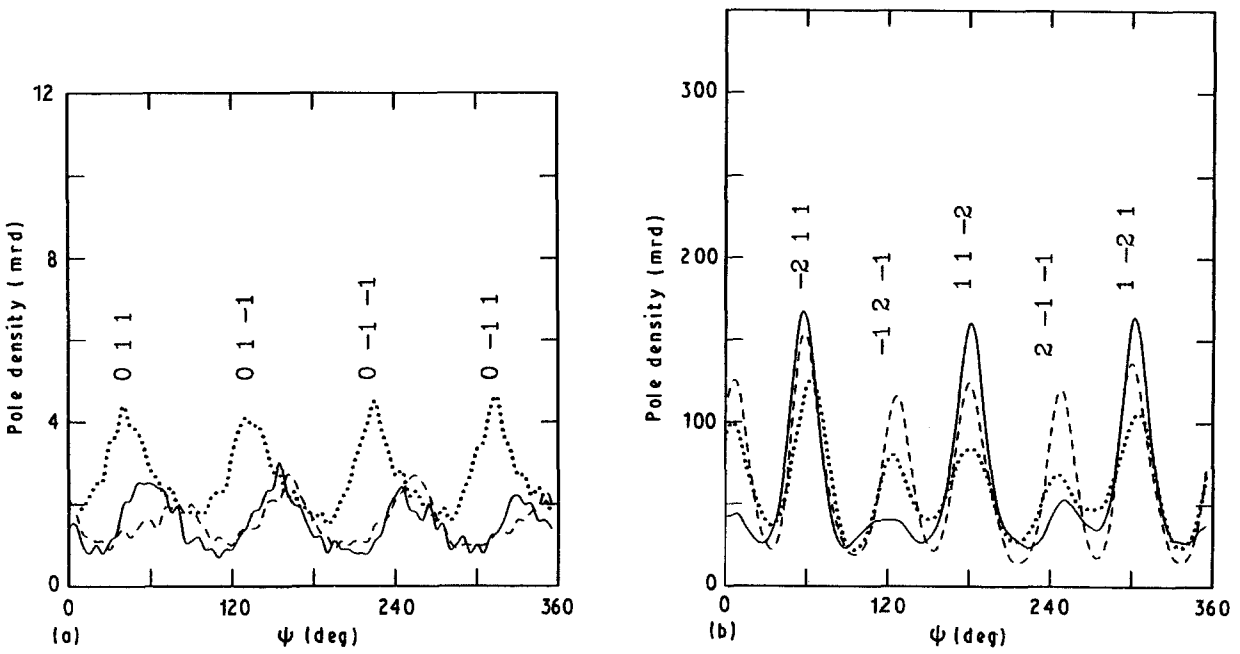


*Figure 7* The (a) (1 0 0) [*u v w*] and (b) (1 1 1) [*u v w*] distributions of the three sections of TaQ2 are presented as a function of the ψ-angles. The Miller indices of the [*u v w*] corresponding to the peak orientations in each distribution are included. (——) S1, (---) S2, (···) S4.

TABLE I Summary of the major texture components found in the tantalum samples, and the corresponding pole densities in mrd unit

| (*hkl*)[*uvw*] | TaPA | TaG1 | TaG2 | TaQ2-S1 | TaQ2-S2 | TaQ2-S4 |
|---|---|---|---|---|---|---|
| (1 1 1)[$\bar{2}$ 1 1] | | | | 160 | 140 | 100 |
| (1 1 1)[2 $\bar{1}$ $\bar{1}$] | | | | 40 | 120 | 80 |
| (1 1 1)[$\bar{3}$ 2 1] | 7 | | | | | |
| (1 1 1)[$\bar{2}$ 3 $\bar{1}$] | 4 | | | | | |
| (1 1 1)[$\bar{1}$ 3 $\bar{2}$] | 3 | | | | | |
| (1 1 1)[$\bar{3}$ 1 2] | 2 | | | | | |
| (1 1 1)-fibre | 2 | 12 | 12 | 20 | 15 | 20 |
| (0 1 4)[1 0 0] | 7 | | | | | |
| (0 1 4)[0 4 $\bar{1}$] | 2 | | | | | |
| (1 0 0)[0 1 0] | 5 | 5 | 12 | | | |
| (1 0 0)[0 4 1] | 4 | | | | | |
| (1 0 0)[0 1 1] | 4 | | | | | 5 |
| (1 0 0)[0 3 2] | 3 | | | 3 | 3 | |
| (1 0 0) fibre | 2 | 7 | 7 | | | |

Fig. 7. The distributions contained a small amount of the [1 0 0] fibre components, estimated to be about 2 mrd for the S4 section, and not more than 1 mrd for the other two sections.

## 5. Discussion

The texture and recrystallization behaviour of rolled tantalum single crystals has been studied by Vandermeer and Snyder [10], for three initial orientations (1 0 0) [0 1 1], (1 1 2) [1 $\bar{1}$ 0] and (1 1 1) [1 $\bar{1}$ 0]. They found that the (1 0 0) [0 1 1] and (1 1 2) [1 $\bar{1}$ 0] were crystallographically stable during rolling and showed no tendency of recrystallization up to 1400 °C, whereas the (1 1 1)[1 $\bar{1}$ 0] reoriented during rolling, and recrystallized easily. The major texture components found in this study are summarized in Table I for comparison. The (1 1 1)⟨1 $\bar{1}$ 0⟩ orientation densities were higher than the random distributions for all the samples in this study, but only as a part of the [1 1 1] fibre type in each sample. The (1 0 0)⟨0 1 1⟩ texture was strong in the TaQ2-S4 and TaPA samples, and also in the TaG type samples as a component of the ⟨1 0 0⟩ fibre texture. However, the (1 1 2)⟨1 $\bar{1}$ 0⟩ were considerably less than the random intensity in all the tantalum samples of the present study.

The commercial tantalum sheet (TaPA) had many texture components as shown in Table I, which reflects the complicated deformation history. On the other hand, the samples obtained by uniaxial compression showed very strong and simple texture. The two TaG-type samples which were obtained from the powder-metallugical ingot had essentially identical texture. However, the textures of the two TaG-type samples were clearly different from that of TaQ2. The major texture components of the TaG type were [1 1 1]/[1 0 0] double fibre with the fibre axes parallel to the compression direction, while those of TaQ2 were a hybrid texture consisting of the [1 1 1] fibre type and the extremely strong (1 1 1)⟨$\bar{2}$ 1 1⟩ and

TABLE II A comparison of the texture indices of the two TaG-type samples and the three sections of TaQ2. The peak intensity of the (1 1 1) and (1 0 0) pole figures (in mrd units) measured at the ND, were also compared

| Sample | T-index | P(1 1 1) | P(1 0 0) |
|---|---|---|---|
| TaG1 | 2.4 | 14.9 | 6.9 |
| TaG2 | 2.5 | 15.2 | 10.4 |
| TaQ2-S1 | 4.6 | 57.7 | 0.4 |
| TaQ2-S2 | 6.1 | 69.6 | 0.7 |
| TaQ2-S4 | 5.7 | 54.4 | 0.9 |

$(1\,1\,1)\langle 2\bar{1}\bar{1}\rangle$ sheet-type texture. The degree of texture was much larger for the TaQ2 samples, with the texture index (integral of the square of the ODF) of 4.6 for TaQ2-S1 and 5.7 for TaQ2-S4 compared to about 2.5 for both of the TaG-type samples, as compared in Table II. The maximum pole density of the (1 1 1) and (1 0 0) pole-figures measured at the ND of both types of sample, are also compared in the table. Considering the fact that their fabrication processes are almost identical, part of the reason for the different textures may be attributed to the different grain-sizes in the original ingots (i.e. much smaller grain-size for the TaG type).

The TaQ2 samples have an extremely strong and well-defined texture, and exhibit a clear mirror symmetry about the RD axis which is consistent with the radial plastic flow in the plane-strain compression, as demonstrated by the pole figures in Fig. 6. It is interesting to notice that the pole figures of the TaQ2 change from pseudo three-fold symmetry at the S1 section to pseudo six-fold symmetry at the S4 section. The texture of the S4 section has pseudo-mirror symmetry about the TD in addition to the symmetry about the RD, which gives a pseudo six-fold symmetry to the pole figures. This difference suggests that the plastic flow in the uniaxial compression is changing with radial distance. Because the amount of radial strain, in the friction-free plane-strain compression, increases linearly with the radial distance, the plastic flow could also change accordingly. It is known that the $(1\,1\,1)[uvw]$ type preferential orientation is the most desirable texture for the deep-drawing fabrication process because it resists through-thickness thinning [11]. In this context, it is worth emphasizing that the ND of the TaQ2 sample is completely dominated by the 1 1 1 orientation.

## References


1. R. K. GARRETT Jr and J. B. CLARK, NSWC TR 88–30 (1988) classified.
2. J. B. CLARK and R. K. GARRET Jr, NSWC TR 88–104 (1989) classified.
3. T. L. JUNGLING, R. K GARRETT Jr and J. B. CLARK, NSWC TR 88–106 (1989) classified.
4. C. S. CHOI, H. J. PRASK and S. F. TREVINO, *J. Appl. Crystallogr.* **12** (1979) 327.
5. J. S. KALLEND, U. F. KOCKS, A. D. ROLLETT and H.-R. WENK, *Mater. Sci. Engng*, **A132** (1991) 1.
6. H. J. BUNGE, *Z. Metallkde* **56** (1965) 872.
7. R. J. ROE, *J. Appl. Phys.* **36** (1965) 2024.
8. S. MATTHIES, H.-R. WENK G. W. VINEL, *J. Appl. Crystallogr.* **21** (1988) 285.
9. U. F. KOCKS, in "ICOTOM-8", edited by J. S. Kallend and G. Gottstein (Metallurgical Society, Warrendale, PA, 1988) p. 31.
10. R. A. VANDERMEER and W. B. SNYDER Jr, *Metall. Trans.* **10A** (1979) 1031.
11. J. B. CLARK, R. K. GARRETT Jr, T. L. JUNGLING, R. A. VANDERMEER and C. L. VOLD, *ibid.* **22A** (1991) 2039.



*Received 27 April*
*and accepted 19 November 1992*